

Tunable caustic phenomena in electron wavefields



Amir Hossein Tavabi^{a,*}, Vadim Migunov^a, Christian Dwyer^a, Rafal E. Dunin-Borkowski^a, Giulio Pozzi^{a,b}

^a Ernst Ruska-Centre for Microscopy and Spectroscopy with Electrons (ER-C) and Peter Grünberg Institute (PGI), Forschungszentrum Jülich, D-52425 Jülich, Germany

^b Department of Physics and Astronomy, University of Bologna, Viale B. Pichat 6/2, 40127 Bologna, Italy

ARTICLE INFO

Article history:

Received 14 January 2015

Received in revised form

6 April 2015

Accepted 9 April 2015

Available online 22 May 2015

Keywords:

Caustics

Transmission electron microscopy

Electron optics

Shaped electron beams

ABSTRACT

Novel caustic phenomena, which contain fold, butterfly and elliptic umbilic catastrophes, are observed in defocused images of two approximately collinear oppositely biased metallic tips in a transmission electron microscope. The observed patterns depend sensitively on defocus, on the applied voltage between the tips and on their separation and lateral offset. Their main features are interpreted on the basis of a projected electrostatic potential model for the electron-optical phase shift.

© 2015 Elsevier B.V. All rights reserved.

1. Introduction

Although they are ubiquitous in nature, optical caustics are intriguing phenomena that play an important role in fundamental and applied optics. In ray optics, caustics can be defined as those points in a wavefield where there is a coalescence of optical rays. At these points, ray optics predicts infinite intensity. In a wave picture, such divergences are tamed and caustics tend to correspond to points of high, but not infinite, intensity. The intensity in the vicinity of a caustic may exhibit complex interference effects, with correspondingly complex patterns occurring in the underlying optical phase (e.g., phase dislocations and vortices). Surprisingly, despite the vast continuum of variations that can be made within an optical system, theoretical considerations show that a discrete classification of caustics is possible using catastrophe theory (see the papers of Berry [1,2] and the book of Nye [3] for a detailed review).

In electron optics, caustic patterns have been observed and utilized for many years in the transmission electron microscope (TEM) [4]. For example, they have been used to characterize quadrupole magnets in terms of electromagnetic lens focus [5], to study time-dependent magnetic fields [6], to measure lens aberrations [7] and to correct astigmatism [8], coma [9] and third-order aberration [10,11]. They have also been used to produce electron vortex beams [12] and Airy beams [13] in the TEM. Simple

caustic phenomena have recently been observed in defocused bright-field TEM images of electrically biased carbon nanotubes [14–17] and metallic tips [18]. In the latter experiments, the tips were biased electrically with respect to significantly larger counter-electrodes and attention was focused on measurements of the electric fields surrounding them.

Here, we present a study of new caustic phenomena, which are formed by electron waves in vacuum and observed in defocused bright-field TEM images of two oppositely biased metallic tips. We show that these caustics can be controlled in a systematic way by varying the potential difference between the metallic tips, their relative positions and/or the image defocus. We also demonstrate good agreement between our experimental results and image simulations based on an idealized model of the electron-optical phase shift induced by the tips.

This paper is organized as follows. In Section 2, we describe our experimental setup. In Section 3, we begin by presenting results obtained when the image defocus is kept constant and the potential difference between the tips is varied. We then keep the potential difference constant and vary the defocus. In Section 4, we describe the theory used for our image simulations. In Section 5, the simulations are used to interpret our experimental results, including a description of the observed interference effects, using the language of catastrophe theory [3]. A discussion and conclusions are presented in Section 6.

* Corresponding author. Fax: +49 2461616444.

E-mail address: a.tavabi@fz-juelich.de (A.H. Tavabi).

2. Experimental details

Two electrochemically etched needle-shaped tungsten tips were mounted in a NanoFactory scanning tunneling microscopy (STM) specimen holder, which comprises a micro-STM setup at the end of a single-tilt TEM specimen holder, as shown in Fig. 1(a). The holder, which is equipped with a piezo-driven STM tip and a sample mount, was used to apply a potential difference between the tips, as shown in Fig. 1(b). The potential difference between the tips, which were approximately collinear, set to be at the same height and observed out-of-focus, was used to create an electric field in the space surrounding them, which acted as a phase object for the electron beam. Interference patterns were recorded in the form of highly defocused bright-field images using an FEI Titan 60–300 TEM equipped with a high-brightness field emission electron gun, a Lorentz lens, a Gatan imaging filter and a 2048 × 2048 pixel charge-coupled device (CCD) camera. The microscope was operated at an accelerating voltage of 300 kV using non-standard lens excitations to provide an optimally wide field of view with high coherence and brightness. A schematic diagram of the setup is shown in Fig. 1(c).

3. Experimental results

3.1. Effect of potential difference at constant defocus

Fig. 2(a) shows a defocused bright-field TEM image of the two tips, for a separation between the ends of the tips of 0.9 μm and a nominal image defocus of −7 mm (i.e., underfocus, with the objective lens of the microscope focused above the specimen),

initially without a voltage applied between the tips. In this image, only Fresnel diffraction fringes around the two opaque tips are visible. The fact that the fringes around the tips have the same spacings confirms that the tips are at the same height in the microscope. Fig. 2(b) shows that an overlapping region is formed at the position of the negatively biased tip when a voltage of 40 V is applied between the tips. This region contains two-beam interference fringes inside it and a two-winged caustic at its end. In contrast, the wavefield at the position of the positively biased tip simply shows an enlarged shadow surrounded by diffraction fringes. The two regions of the wavefield look similar to those observed for a single tip in front of a planar electrode [18] and, at this stage, interact with each other weakly. Even though Fig. 2 (b) was recorded at the same defocus as Fig. 2(a) without changing the settings of the projector lenses in the microscope, there is a slight change in magnification and a shift between the two images. The latter changes are thought to arise from the non-standard lens settings used, as well as from small changes in the excitations of the condenser lenses in the microscope. As a result of such unknown changes in magnification and image shift, scale bars are shown only for simulations and not for experimental images below.

Fig. 2(c) shows that the overlapping region at the position of the negatively biased tip widens and the two-beam interference fringe spacing decreases when the applied voltage is increased to 60 V. In addition, the two defocused images begin to interact, resulting in the creation of two high-contrast folds, with an increase in intensity and a fringe modulation where they cross. When the applied voltage is increased further to 100 V, a butterfly-like pattern develops, as shown in Fig. 2(d).

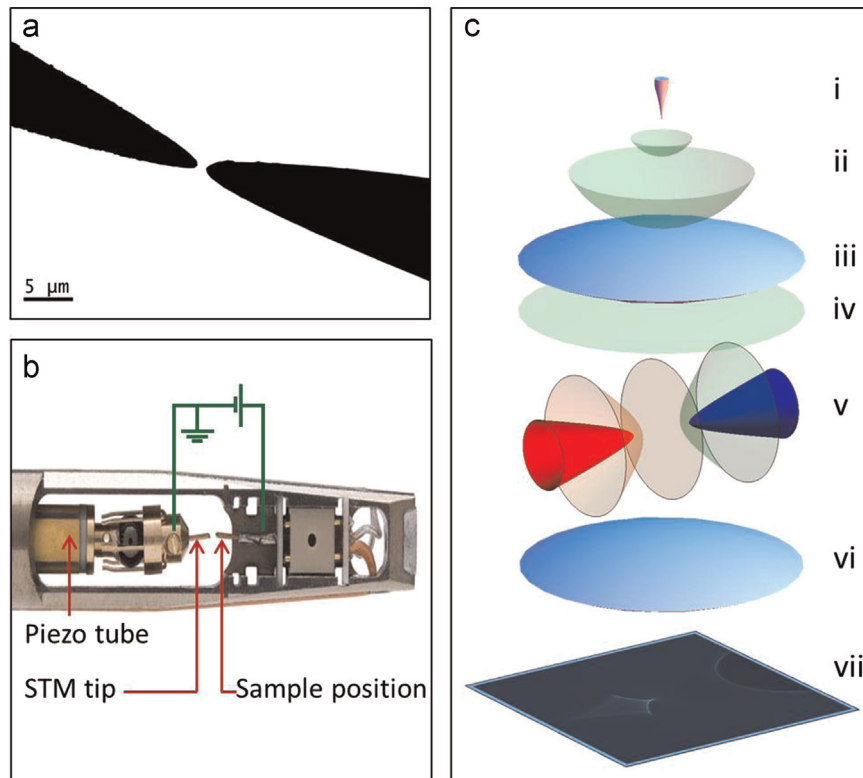


Fig. 1. Experimental setup. (a) Low-magnification bright-field TEM image of two electrochemically etched needle-shaped tungsten tips used to produce caustics in the TEM. (b) Photograph of the end of a NanoFactory STM specimen holder, in which the two tips were mounted on the STM tip and sample mount before inserting the holder into the TEM. (c) Schematic diagram of the electron-optical setup in the TEM, including (i) a field emission electron gun, (ii) a spherical incident electron wave, (iii) the condenser lens system of the microscope, (iv) a plane electron wave, (v) the biased tungsten tips, (vi) the magnifying lens system of the microscope and (vii) a bright-field TEM image recorded on a CCD camera.

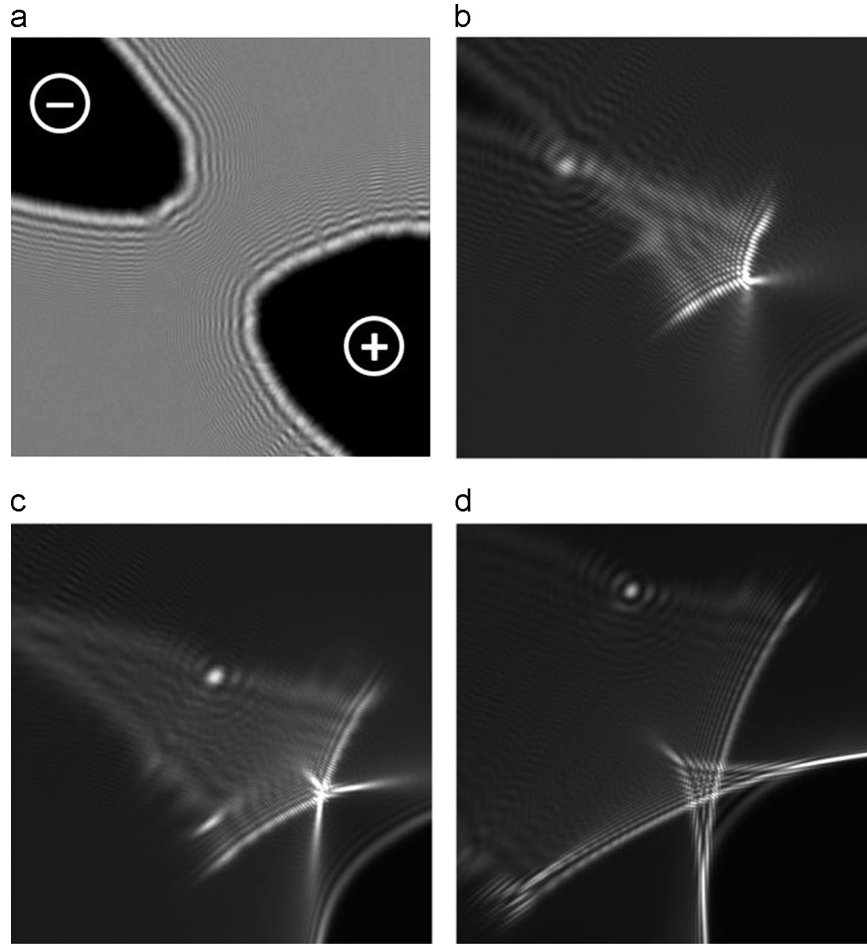


Fig. 2. Defocused bright-field TEM images of the two tungsten tips recorded at a constant defocus of -7 mm. The potential difference between the tips is (a) 0, (b) 40, (c) 60 and (d) 100 V. The white dot visible in (b), (c) and (d) probably arises from a small region of contamination on one of the tips.

3.2. *Effect of defocus at constant potential difference*

The interaction between the images of the two tips is better appreciated when the experiment is carried out at a fixed potential difference, while varying the image defocus. Fig. 3 shows results obtained for a potential difference of 130 V and defocus values of between -3 and -8 mm. After the caustic around the negatively biased tip grows in Fig. 3(a) and (b), a triangular structure becomes visible at the crossing of the two folds in Fig. 3(c) and increases in size with increasing defocus in Fig. 3(d) and (e). This triangular structure is linked to two protruding butterfly-like wings, from which it separates into an isolated triangular structure that is reminiscent of an elliptic umbilic catastrophe [3]. It is interesting that a triangular caustic (and especially an elliptic umbilic-like catastrophe) can be formed by electrons that have only passed two approximately collinear biased metallic tips. We show below how the structure of the elliptic umbilic-like catastrophe can be displayed fully by varying the tip separation.

4. **Theoretical considerations**

4.1. *Model for the potential and the phase shift*

A theoretical model was developed based on an existing analytical description of the electrostatic potential and electron-optical phase shift associated with two biased metallic tips [19]. The model is based on a line charge in front of a conducting plane and makes use of the method of images. As the equipotential surfaces

around two line charges are ellipsoids, which are in turn similar to the physical shapes of the metallic tips in our experiments, in principle two opposite lines of charge generate a suitable solution for the potential in the region surrounding and between the tips. Unfortunately, this model is not quite sufficient to represent the present experimental setup, as the two tips are only approximately (and not exactly) aligned laterally. A more versatile model, which is described below, was therefore developed.

The starting point is the electrostatic potential distribution associated with two opposite infinitesimal point charges, $\pm dq$, one located at a variable position $(0, y_0, 0)$ (where the z -axis is parallel to and in the same direction as the electron beam) and the other at a fixed position $(-x_D, -y_D, 0)$. The role of the second charge is to ensure overall charge neutrality and therefore convergence of the projected potential. The potential arising from the point charges is given by the expression

$$dV(x, y, z) = \frac{dq}{4\pi\epsilon_0} \left(\frac{1}{\sqrt{x^2 + (y - y_0)^2 + z^2}} - \frac{1}{\sqrt{(x + x_D)^2 + (y + y_D)^2 + z^2}} \right). \quad (1)$$

The equation for the electron-optical phase shift takes the form

$$\varphi(x, y) = C_E \int_{-\infty}^{\infty} V(x, y, z) dz, \quad (2)$$

where C_E is an interaction constant that takes a value of 6.53×10^6 rad V $^{-1}$ m $^{-1}$ for 300 kV electrons [17–19]. By combining Eqs. (1) and (2), the contribution to the phase shift from the two point charges can be written as

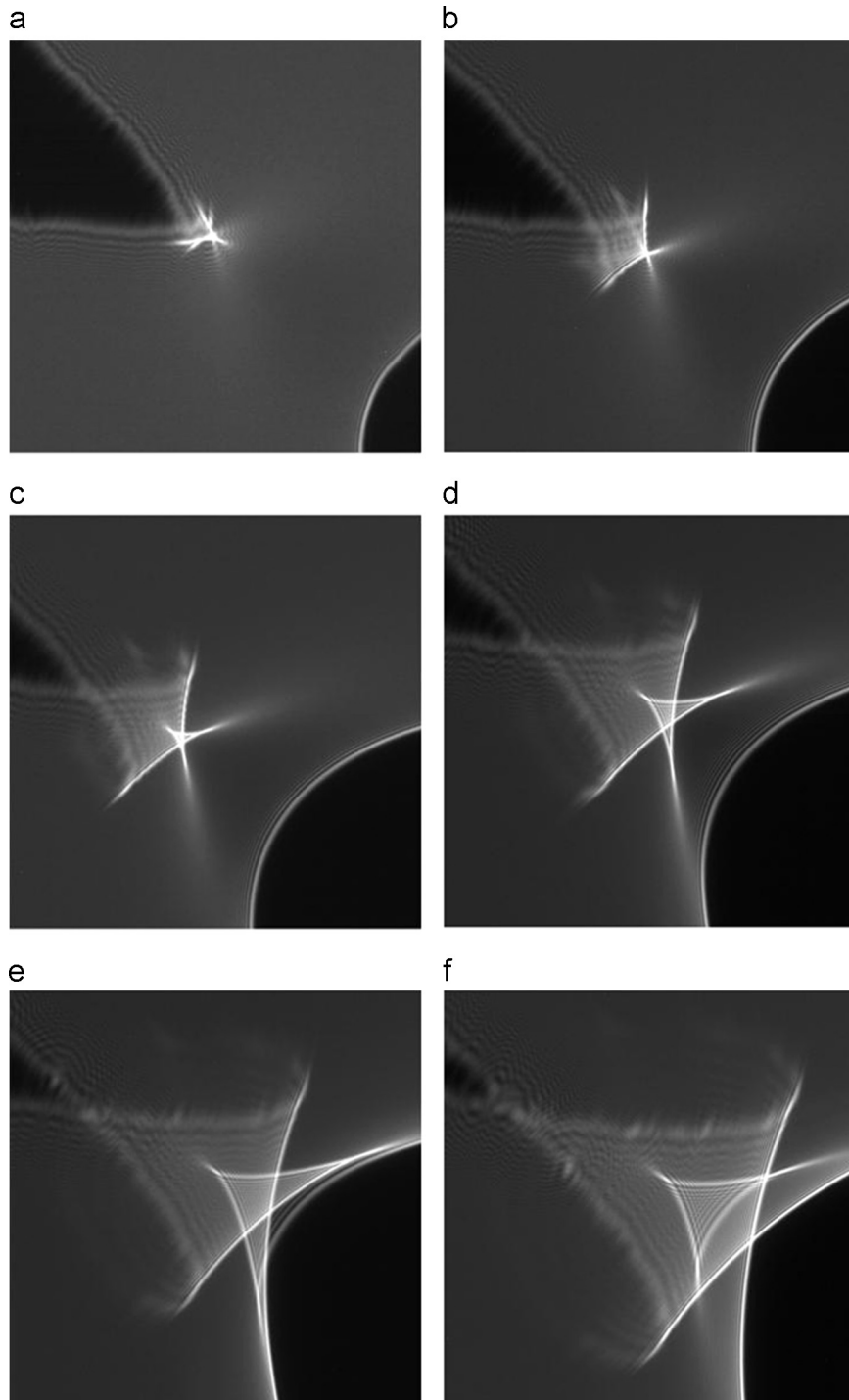


Fig. 3. Defocused bright-field TEM images of the two tungsten tips recorded at a constant potential difference between them of 130 V. The defocus is (a) –3, (b) –4, (c) –5, (d) –6, (e) –7 and (f) –8 mm.

$$d\varphi(x, y) = \frac{C_E dq}{4\pi\epsilon_0} \left[\log((x + x_D)^2 + (y + y_D)^2) - \log(x^2 + (y - y_0)^2) \right]. \quad (3)$$

If the charge density is assumed to be constant along y , then $dq = K dy_0$, where K is a constant with units of charge density. Integration of Eq. (1) with respect to y_0 from $-a$ to 0 provides an analytical expression for the total potential, which is given in the

$z=0$ plane by

$$V(x, y) = \frac{K}{4\pi\epsilon_0} \left[\log \left(\frac{\sqrt{(a+y)^2 + x^2} + a + y}{\sqrt{x^2 + y^2} + y} \right) - \frac{a}{\sqrt{(x + x_D)^2 + (y + y_D)^2}} \right]. \quad (4)$$

By defining

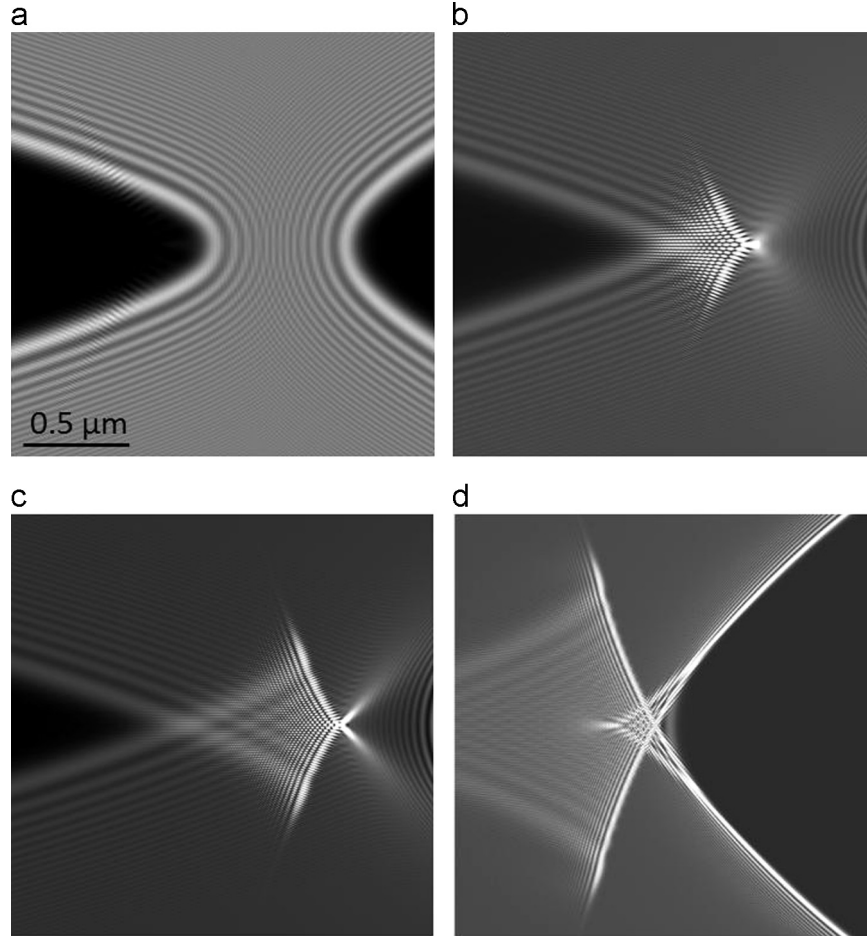


Fig. 4. Simulated defocused bright-field TEM images of the two tips for a constant defocus of -7 nm. The potential difference between the tips is (a) 0, (b) 40, (c) 60 and (d) 100 V. The tip separation is $0.9 \mu\text{m}$.

$$C_V = \frac{K}{4\pi\epsilon_0}, \quad (5)$$

the final equation for the phase shift is

$$\begin{aligned} \varphi(x, y) = C_V C_V \left[& -(a + y) \log((a + y)^2 + x^2) \right. \\ & + y \log(x^2 + y^2) + 2a + 2x \tan^{-1}\left(\frac{y}{x}\right) \\ & - 2x \tan^{-1}\left(\frac{a + y}{x}\right) + a \log((x + x_D)^2 \\ & \left. + (y + y_D)^2) \right]. \quad (6) \end{aligned}$$

Any combination of line charges of constant charge density can be described by rotating and displacing the above expressions relative to a single line charge. In particular, by taking two line charges of equal length, the total charge is zero and there is no longer a need to introduce compensating charges at large distances.

4.2. Simulation of defocused images

Out-of-focus images that are formed by illuminating a specimen using a coherent electron beam can be simulated by calculating the image wavefunction in the observation plane (X, Y, Z) using the Kirchhoff–Fresnel integral:

$$\begin{aligned} \psi(X, Y, Z) = \frac{\exp(i\beta)}{\lambda Z} \iint A(x, y) \exp\left\{ \frac{i\pi}{\lambda Z} [(x - X)^2 \right. \\ \left. + (y - Y)^2 + \varphi(x, y)] \right\} dx dy, \quad (7) \end{aligned}$$

where λ is the deBroglie wavelength of the incident electrons and β is a phase factor that is unimportant here as only the intensity in the image plane, which is proportional to $|\psi|^2$, is relevant. $A(x, y)$ is an amplitude function, which is used to describe the fact that the tips are not transparent to the electron beam. Plane wave illumination is assumed.

We calculated the Kirchhoff–Fresnel integral using Fourier-transform-based methods for square regions of side $4.096 \mu\text{m}$ using 2048×2048 sampling points and for square regions of side of $8.192 \mu\text{m}$ using 4096×4096 sampling points. A lateral offset of $2 \mu\text{m}$ between the center of the image and the tips was introduced and a linear phase term was subtracted from the phase shift in order to minimize artifacts due to boundary conditions. Additional test calculations were carried out using twice the dimensions and double the number of sampling points and showed no significant differences.

In order to calculate the amplitude and phase of the transmission function of the two tips, the following procedure was adopted. By plotting the equipotential surfaces in the object plane using Eq. (4) with $C_V = 1$, the values of potential that best fitted the shapes of the two tips were chosen. By considering the tips to be completely opaque to electrons, the amplitude $A(x, y)$ was chosen to be zero for values of potential inside the tips and unity outside. The value of C_V was then rescaled so that the potential difference

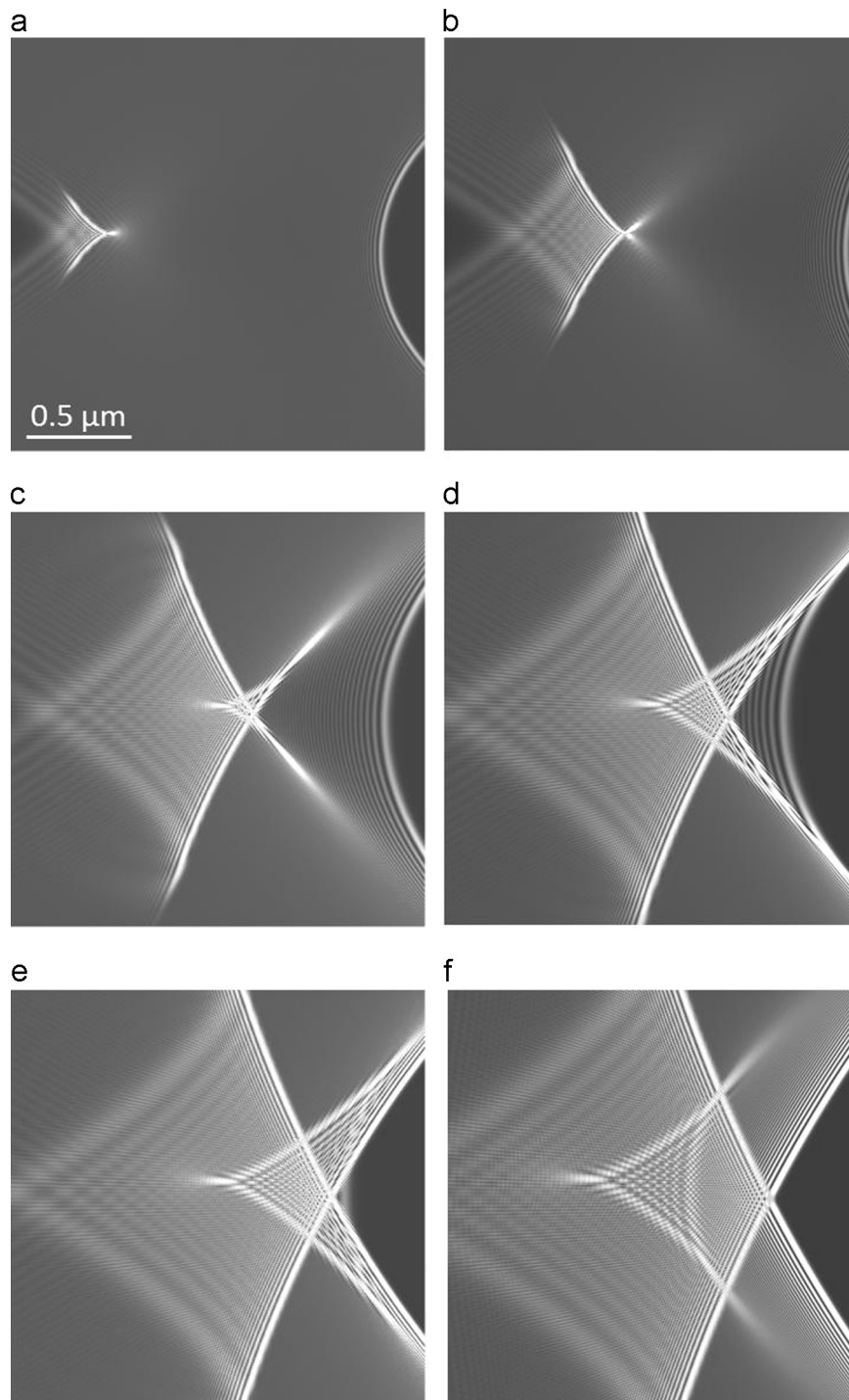


Fig. 5. Simulated defocused bright-field TEM images of the two tips for a constant potential difference of 130 V. The defocus is (a) -3 , (b) -5 , (c) -8 , (d) -10 , (e) -11 and (f) -13 mm. The tip separation is $1.8 \mu\text{m}$ and their lateral offset is $0.1 \mu\text{m}$

corresponded to the experimental value. By inserting this value into the expression for the phase using Eq. (6), the complete transmission function of the object was obtained. (It should be noted that, in the present paper, the parameter a and the lateral offset between the two line charges were chosen on the basis of a visual best fit. An improved fit could be achieved by using an approach similar to that described in Ref. [20].)

5. Interpretation of experimental results

Fig. 4(a)–(d) shows simulated defocused images for the experimental conditions used in Fig. 2, i.e., for a constant defocus of

-7 mm and different values of potential difference between the tips. The amplitude function was calculated by taking values of 3.5 V and -2.5 V for the potentials of the tips ($C_V=1$), with the two line charges ($20 \mu\text{m}$ in length) aligned and separated by $0.9 \mu\text{m}$. There is a satisfying degree of agreement between the experimental and simulated images.

When corresponding simulations were carried out for a constant potential difference and varying defocus, good agreement was only obtained when defocus values of -3 , -5 , -8 , -10 , -11 and -13 mm were used in Fig. 5(a)–(f), respectively. In this case, the amplitude function was calculated by taking values of 3 V and

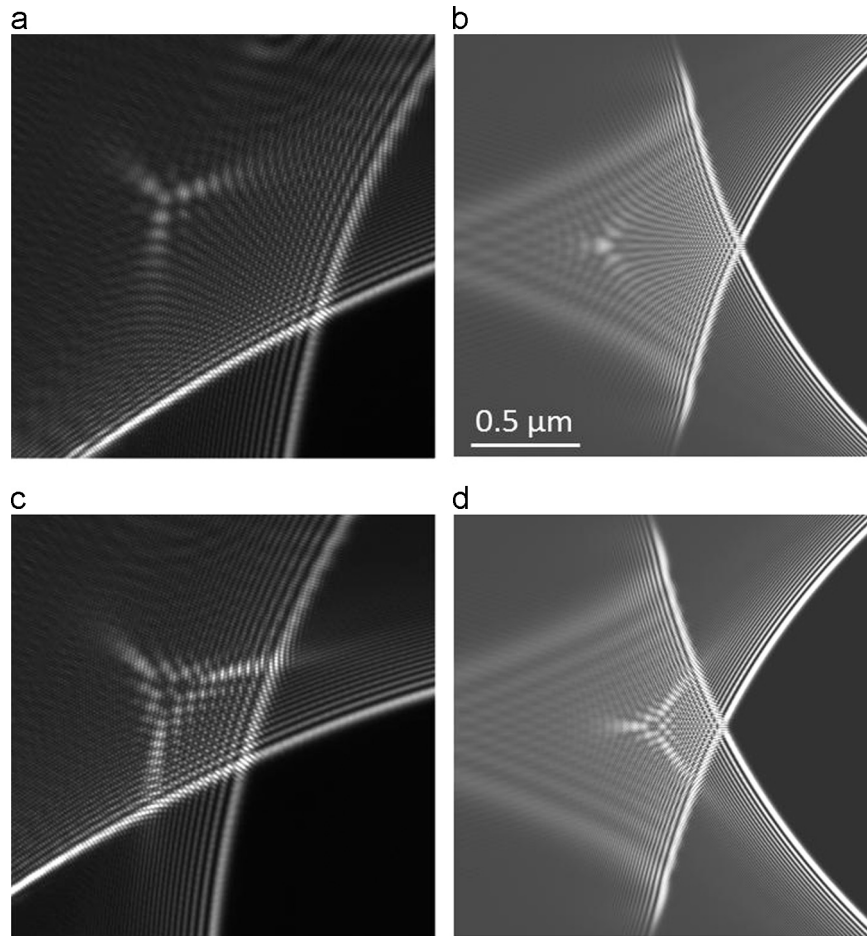


Fig. 6. Experimental defocused bright-field TEM images recorded at a nominal defocus of -9 mm and a potential difference of -80 V for tip separations of (a) 500 and (c) 800 nm. (b) and (d) show simulated images for the experimental conditions in (a) and (c), respectively.

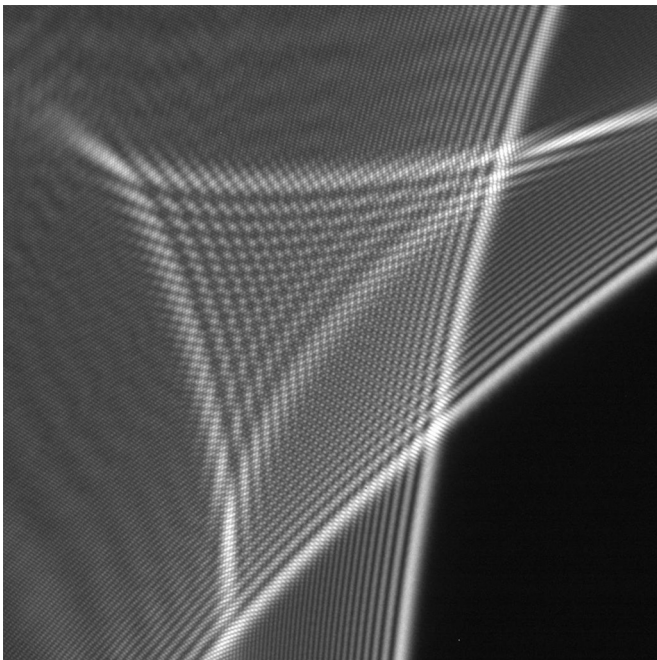


Fig. 7. High-magnification defocused bright-field TEM image of the two tips, corresponding to an enlarged version of Fig. 3(f). The potential difference between the tips is 130 V and the defocus is -8 mm.

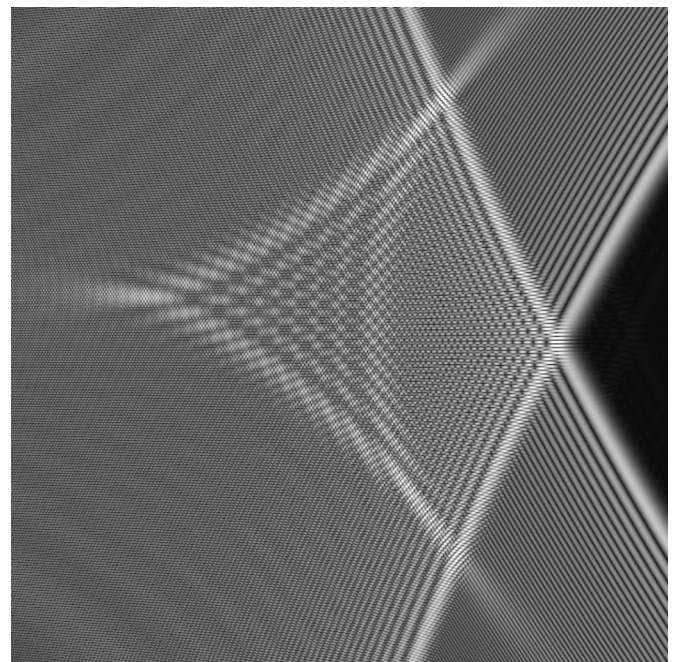


Fig. 8. Simulated defocused bright-field TEM image of the two tips, corresponding to an enlarged version of Fig. 5(f). The potential difference between the tips is 130 V and the defocus is -13 mm. The tip separation is 1.8 μm and their lateral offset is 0.1 μm .

–3 V for the potentials of the tips ($C_V=1$), with the two line charges (60 μm in length) separated by 1.8 μm and using a lateral offset of 0.1 μm to take into account the slight asymmetry of the images. The discrepancy between the experimental and theoretical defocus values is thought to result from two main factors: a lack of calibration of the microscope at the non-standard settings that were used and a lack of fine control over the illumination conditions. As shown in Ref. [21], the influence of spherical (rather than planar) illumination can strongly affect the defocus values and effective magnification of such images. As mentioned above, it is for this reason that scale bars are given only for simulations and not for experimental defocused images here.

In order to emphasize the elliptic umbilic feature in the caustic, we performed an experiment in which the tip separation was varied between values of approximately 500 and 800 nm at a nominal defocus value of –9 mm for an applied voltage of –80 V. The experimental results and corresponding simulations are shown in Fig. 6. For the simulations, the amplitude function was calculated by taking values of 3.5 V and –2.5 V for the potentials of the tips ($C_V=1$), with the two line charges (20 μm in length) aligned and separated by 0.5 and 0.8 μm , as shown in Fig. 6(b) and (d), respectively. Good agreement for the umbilic catastrophe, when compared with the experimental results shown in Fig. 6(a) and (c), is obtained when the defocus is taken to be –10 mm for a potential difference of 80 V, instead of the nominal value of –9 mm. There is a remaining slight discrepancy in the width of the overlapping region, which is not as wide in the simulations as in the experimental images.

The fine structure present in the caustic patterns is illustrated at higher magnification in Fig. 7, which is an enlarged version of Fig. 3 (f). The corresponding simulation, which is an enlarged version of Fig. 5(f), is shown in Fig. 8. The fine structure of the features that modulate the main diffraction image is impressive and indicates that more than four (in fact six) rays contribute to this pattern.

6. Discussion and conclusions

We have shown that novel electron-optical caustic phenomena can be created when two oppositely biased metallic tips are illuminated using highly coherent electrons in a transmission electron microscope. Our experimental setup offers the flexibility to produce and study a wide variety of different caustics, in which very fine structures can be formed as result of the coherence of the incident electron wave. Moreover, it offers the ability to study, in a single experiment, the transformation of simple caustics into more complex ones. Such transformations have been difficult to achieve in previous studies using light, which have employed a single lens, e.g., a water droplet, to produce only a specific caustic.

The key features in our experimental images can be interpreted using a relatively simple electrostatic model based on line charges, in which equipotential surfaces are used to mimic the nearly ellipsoidal shapes of the tips. The qualitative agreement between the experimental and simulated images is very good. Although it has not yet been possible to obtain full quantitative agreement between the experimental and theoretical results, owing in large part to uncertainties in several experimental parameters (e.g., the defocus and illumination conditions), as well as the inability to model the electrode shapes precisely, the good qualitative agreement confirms the soundness of the model.

The interference patterns observed in this work appear to correspond to higher-order caustics, which, for certain values of the control parameters (applied bias and image defocus), undergo degeneration into simpler caustics, such as cusp and elliptic umbilic catastrophes. To the best of our knowledge, the caustic patterns that we have reported here have not been reported previously in the literature.

Work is in progress to relate the underlying phase shifts to the catastrophe interpretation of caustic patterns [3]. The present experiments suggest that controlled shaping of electron beams can be achieved using multiple tips, in order to produce various types of electron beams such as vortex probes and Airy beams.

Acknowledgments

We are grateful to Prof. Michael Farle and his colleagues in the Fakultät für Physik and Center of Nanointegration (CeNIDE), Universität Duisburg-Essen for technical support, to the Deutsche Forschungsgemeinschaft for a Deutsch-Israelische Projektkooperation (DIP) Grant, to the European Commission for an Advanced Grant, to the European Commission for the Marie Curie Initial Training Network (ITN) SIMDALEE2: Grant No. 606988 under FP7- PEOPLE-2013-ITN and to the European Union Seventh Framework Programme for funding under Grant agreement 312483-ESTEEM2 (Integrated Infrastructure Initiative-I3).

References

- [1] M.V. Berry, Waves and Thom's theorem, *Adv. Phys.* 25 (1) (1976) 1–26.
- [2] M.V. Berry, J.F. Nye, F.J. Wright, The elliptic umbilic diffraction catastrophe, *Phil. Trans. R. Soc. Lond. A* 291 (1382) (1979) 453–484.
- [3] J.F. Nye, *Natural Focusing and Fine Structure of Light: Caustics and Wave Dislocations*, Institute of Physics Pub., Bristol, 1999.
- [4] W. Glaser, *Grundlagen der Elektronenoptik*, Springer, Wien, 1952.
- [5] H. Schneider, An A.G. channel with four quadrupole magnets, *Nucl. Instrum. J.* (5) (1957) 268–273.
- [6] D. Laroze, R. Rivera, An exact solution for electrons in a time-dependent magnetic field, *Phys. Lett. A* 355 (4–5) (2006) 348–351.
- [7] E. Wolf, The diffraction theory of aberrations, *Rep. Prog. Phys.* 14 (1) (1951) 95–120.
- [8] Q. Xing, T.A. Lograsso, A rapid method to correct objective lens astigmatism in a TEM, *Ultramicroscopy* 109 (4) (2009) 287–290.
- [9] K. Kimoto, K. Ishizuka, N. Tanaka, Y. Matsui, Practical procedure for coma-free alignment using caustic figure, *Ultramicroscopy* 96 (2) (2003) 219–227.
- [10] K. Kanaya, H. Kawakatsu, Method of measuring spherical and astigmatic aberrations by shadow electron microscope images, *J. Electron Microsc. J.* (1960) 1–3.
- [11] K. Kanaya, E. Oho, K. Adachi, Y. Yamamoto, H. Doi, Caustic patterns combined with second and third order astigmatism in high resolution scanning electron microscopes, *Micron Microsc. Acta* 21 (1–2) (1990) 57–68.
- [12] T. Petersen, M. Weyland, D. Paganin, T. Simula, S. Eastwood, M. Morgan, Electron vortex production and control using aberration induced diffraction catastrophes, *Phys. Rev. Lett.* 110 (3) (2013) 033901.
- [13] N. Voloch-Bloch, Y. Lereah, Y. Lilach, A. Gover, A. Arie, Generation of electron Airy beams, *Nature* 494 (7437) (2013) 331–335.
- [14] B. Cho, T. Ogawa, T. Ichimura, T. Ichinokawa, T. Amakusa, C. Oshima, Low-temperature field emission system for development of ultracoherent electron beams, *Rev. Sci. Instrum.* 75 (10) (2004) 3091–3096.
- [15] T. Kasama, Y. Antypas, R.K.K. Chong, R.E. Dunin-Borkowski, Novel approaches for the characterization of electromagnetic fields using electron holography, *Mater. Res. Soc. Symp. Proc.* 839 (2004) P5.1.1–P5.1.12.
- [16] B. Cho, T. Ishikawa, C. Oshima, Coherent and intense multibeam generation by the apex of sharp nano-objects: electron half-circular prism, *Appl. Phys. Lett.* 91 (16) (2007) 163102.
- [17] M. Beleggia, T. Kasama, R.E. Dunin-Borkowski, S. Hofmann, G. Pozzi, Direct measurement of the charge distribution along a biased carbon nanotube bundle using electron holography, *Appl. Phys. Lett.* 98 (24) (2011) 243101–243103.
- [18] G. Pozzi, M. Beleggia, T. Kasama, R.E. Dunin-Borkowski, Interferometric methods for mapping static electric and magnetic fields, *C. R. Phys.* 15 (2) (2014) 126–139.
- [19] G. Matteucci, G. Missiroli, M. Muccini, G. Pozzi, Electron holography in the study of the electrostatic fields: the case of charged microtips, *Ultramicroscopy* 45 (1) (1992) 77–83.
- [20] M. Beleggia, T. Kasama, D.J. Larson, T.F. Kelly, R.E. Dunin-Borkowski, G. Pozzi, Towards quantitative off-axis electron holographic mapping of the electric field around the tip of a sharp biased metallic needle, *J. Appl. Phys.* 116 (2) (2014) 024305.
- [21] P.F. Fazzini, P.G. Merli, G. Pozzi, Electron microscope calibration for the Lorentz mode, *Ultramicroscopy* 99 (2–3) (2004) 201–209.